AD-A191 600 ANALYSIS OF MOLECULAR MIXING AND CHEMICAL REACTION IN MIXING LAYER.. (U) CALIFORNIA UNIV IRVINE DEPT OF MECHANICAL ENGINEERING B M CETEGEN ET AL. 14 JAN 88 1/1

UNCLASSIFIED AFOSR-TR-88-0242 AFOSR-86-0016 F/G 7/4 NL

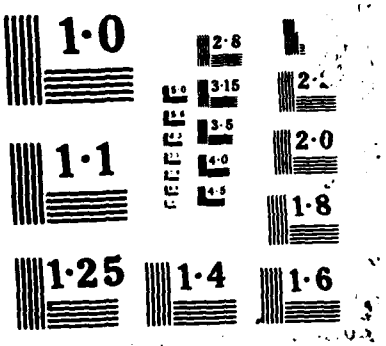
1·0
1·1
1·25
1·4
1·6
2·0
1·8

Unclassified

(2)

AD-A191 600

DTIC ELECTE MAR 1 1 1988 D

REPORT DOCUMENTATION PAGE

DTIC FILE COPY

1b. RESTRICTIVE MARKINGS: None	
2a. SECURITY CLASSIFICATION: Unclassified	3. DISTRIBUTION/AVAILABILITY OF REPORT: Distribution unlimited; approved for public release
2b. DECLASSIFICATION/DOWNGRADING SCHEDULE: Unclassified	
4. PERFORMING ORGANIZATION REPORT NUMBER(S)	5. MONITORING ORGANIZATION REPORT NUMBER(S): AFOSR-TR- 88-0242
6a. NAME OF PERFORMING ORGANIZATION: University of California Dept. of Mechanical Engr.	6b. OFFICE SYMBOL (If applicable)
6c. ADDRESS (City, State and ZIP Code): Irvine, CA 92717	7a. NAME OF MONITORING ORGANIZATION: Air Force Office of Scientific Research
	7b. ADDRESS (City, State and ZIP Code): BLDG 410 Bolling AFB DC 20332-6448
8a. NAME OF FUNDING/SPONSORING ORGANIZATION: Air Force Office of Sci. Res.	8b. OFFICE SYMBOL (If applicable): AFOSR/NA
	9. PROCUREMENT INSTRUMENT IDENTIFICATION NUMBER: AFOSR-86-0016
8c. ADDRESS (City, State and ZIP Code): BLDG 410 Bolling AFB DC 20332-6448	10. SOURCE OF FUNDING NOS.

PROGRAM ELEMENT NO.	PROJECT NO.	TASK NO.	WORK UNIT NO.
61102F	2308	A2	

11. TITLE (Include Security Classification): Analysis of Molecular Mixing and Chemical Reaction in a Mixing Layer

12. PERSONAL AUTHOR(S): B.M. Cetegen and W.A. Sirignano

13a. TYPE OF REPORT	13b. TIME COVERED	14. DATE OF REPORT (Yr., Mo., Day)	15. PAGE COUNT
Publication	FROM 10/86 TO 10/87	January 11-14, 1988	7

16. SUPPLEMENTARY NOTATION

17. COSATI CODES			18. SUBJECT TERMS (Continue on reverse if necessary and identify by block number)
FIELD	GROUP	SUB. GR.	Turbulent Reacting Flows; Molecular Mixing and Reaction in Vortical Structures

19. ABSTRACT (Continue on reverse if necessary and identify by block number)

This paper concerns an analytical study of molecular mixing and finite rate chemical reactions in an infinite row of vortices representing a mixing layer. Diffusion equations for reacting and non-reacting species are solved locally in the Lagrangian frame of reference following material elements. The flowfield is a given for the problem. The concentration distributions in the vortex structure are composed from these analytical solutions and presented for several cases. The probability density functions constructed from these distributions are compared with the mixing layer experiments. For the cases studied, the comparisons indicate encouraging agreement for the reacting flow case. However, some differences are present for the non-reacting flows.

20. DISTRIBUTION/AVAILABILITY OF ABSTRACT	21. ABSTRACT SECURITY CLASSIFICATION
UNCLASSIFIED/UNLIMITED ☒ SAME AS RPT. ☒ DTIC USERS ☒	Unclassified

22a. NAME OF RESPONSIBLE INDIVIDUAL	22b. TELEPHONE NUMBER (Include Area Code)	22c. OFFICE SYMBOL
Julian M. Tishkoff	(202) 767-4965	AFOSR/NA

DD FORM 1473, 83 APR EDITION OF 1 JAN 73 IS OBSOLETE.

Unclassified
SECURITY CLASSIFICATION OF THIS PAGE

AIAA'88

AIAA-88-0730

Analysis of Molecular Mixing and Chemical Reaction in a Mixing Layer

B.M. Cetegen and W.A. Sirignano
University of California
Irvine, CA

AIAA 26th Aerospace Sciences Meeting
January 11-14, 1988/Reno, Nevada

ANALYSIS OF MOLECULAR MIXING AND CHEMICAL REACTION IN A MIXING LAYER

by

B.M. Cetegen and W.A. Sirignano
University of California
Irvine, California 92717

ABSTRACT

This paper concerns an analytical study of molecular mixing and finite rate chemical reactions in an infinite row of vortices representing a mixing layer. Diffusion equations for reacting and non-reacting species are solved locally in the Lagrangian frame of reference following material elements. The flowfield is a given for the problem. The concentration distributions in the vortex structure are composed from these analytical solutions and presented for several cases. The probability density functions constructed from these distributions are compared with the mixing layer experiments. For the cases studied, the comparisons indicate encouraging agreement for the reacting flow case. However, some differences are present for the non-reacting flows.

INTRODUCTION

In many combustion systems, the combustion of fuel and oxidizer takes place in turbulent flow reactors where fuel and oxidizer, in either premixed or non-premixed form, are introduced into a mixing zone. Since chemical reactions take place upon molecular mixing of reactants, there is a strong interaction between the combustion processes and the local flowfield. A typical example is the reacting mixing layer behind a splitter plate separating the fuel and oxidizer streams that meet at the plate's trailing edge. In general, the two streams have different speeds to promote mixing of the reactants, thus the combustion rate. In such a flow configuration, well-known initially two dimensional vortices are formed due to the onset of the Kelvin-Helmholtz instability. This problem has received vast amount of attention in the past several decades. Experimental studies on non-reacting and reacting shear layers[1,2,3,4] have been complemented by elaborate numerical simulations of this flow configuration[5,6,7]. The references cited here are just a few examples of many in the literature. These studies have made significant contributions to our understanding of these technologically important flowfields.

In numerical simulation of reacting flows, computations must be performed that resolve small length scales (of the order of the diffusive length scales) to predict molecular mixing and chemical reactions. This level of resolution, in general, requires very time consuming and expensive calculations. At the same time, some methods, such as finite difference simulations, are hindered by the numerical diffusion errors which need to be eliminated by elaborate and computer time intensive numerical methods.

The problem considered here is an approximate analytical approach to solve the mixing problem in a mixing layer imbedded with a line of two dimensional vortices. This situation approximates the temporal growth of a mixing layer locally without the effect of pairing. In this paper, the mixing and reaction of two initially segregated species streams are analyzed in a Lagrangian frame of reference accounting for the stretching of the material lines as molecular diffusion and chemical reactions are taking place across them. This approach follows the methodology of Marble[8] and Marble and Karagozian[9] in that the study of the local behavior does provide an accurate representation of the local physical processes. This approach was recently used by Cetegen and Sirignano[10] to determine the concentration field of non-reacting and reacting scalars within a two-dimensional single vortex and its mixing statistics. In this paper, this technique is extended to the study of an infinite row of vortices which exhibit some differences with respect to the strain field.

In the following, the method of analysis is first outlined. The approximate treatment of the finite rate chemical reactions between the two reactive species is described. The concentration distributions and mixing statistics are presented and discussed in the results section.

METHOD OF ANALYSIS

Flowfield

The computation of the concentration field within an infinite row of vortices relies on the knowledge of the flowfield. The velocity field is utilized to calculate the successive positions of the material elements in time as well as the strain rates experienced by them. This facilitates analytical solution for the concentration profiles about the material elements locally. In this paper, the velocity distribution for an infinite row of point vortices is modified to include a viscous core in the center of each vortex. The velocity distribution for an infinite row of point vortices[11] is given by

$$u = \left(\frac{\Gamma}{2a}\right) \frac{\operatorname{Sinh}\left(\frac{2\pi y}{a}\right)}{\operatorname{Cosh}\left(\frac{2\pi y}{a}\right) - \operatorname{Cos}\left(\frac{2\pi x}{a}\right)} \qquad (1a)$$

$$v = \left(\frac{-\Gamma}{2a}\right) \frac{\operatorname{Sin}\left(\frac{2\pi x}{a}\right)}{\operatorname{Cosh}\left(\frac{2\pi y}{a}\right) - \operatorname{Cos}\left(\frac{2\pi x}{a}\right)} \qquad (1b)$$

The coordinate system and the parameters in these equations are depicted in Figure 1. The velocity distribution represented by Equation (1) represents a horizontal velocity jump of magnitude Γ/a, from $-\Gamma/2a$ to $+\Gamma/2a$. Since the tangential velocity at the center of a potential point vortex tends to infinity, a situation which is not realized in viscous fluids, we can

incorporate the effects of viscosity by introducing a time dependent viscous core given by a Rankine vortex.

Since the problem is periodic in the x direction, we can consider one of the vortices under the influence of semi-infinite rows of vortices on each side. In particular, if we confine our attention to the vortex situated at x = 0, y = 0, then the velocity field can be obtained by superposition of a viscous core yielding,

$$u = \left(\frac{\Gamma}{2a}\right) \frac{\text{Sinh}\left(\frac{2\pi y}{a}\right)}{\text{Cosh}\left(\frac{2\pi y}{a}\right) - \text{Cos}\left(\frac{2\pi x}{a}\right)} - \left(\frac{\Gamma}{2\pi}\right) \frac{y}{x^2 + y^2} e^{-\frac{x^2 + y^2}{4\nu t}} \qquad (2a)$$

$$v = \left(\frac{-\Gamma}{2a}\right) \frac{\text{Sin}\left(\frac{2\pi y}{a}\right)}{\text{Cosh}\left(\frac{2\pi y}{a}\right) - \text{Cos}\left(\frac{2\pi x}{a}\right)} + \left(\frac{\Gamma}{2\pi}\right) \frac{x}{x^2 + y^2} e^{-\frac{x^2 + y^2}{4\nu t}} \qquad (2b)$$

The superposition is valid in the potential flow region outside the viscous core and is approximate in the core region. However, this approximation is admissable in view of the fact that most of the straining occurs in the potential region outside the viscous core.

Molecular Diffusion

In this flowfield, a material surface initially coincident with the horizontal x-axis, undergoes a distortion. Across this material surface separating the two species, molecular diffusion takes place as this interface is stretched and transported in the vortex field. The species diffusion equation for a locally planar interface can be written as

$$\frac{\partial C}{\partial t} + \bar{u}\frac{\partial C}{\partial \bar{x}} + \bar{v}\frac{\partial C}{\partial \bar{y}} = D\left(\frac{\partial^2 C}{\partial \bar{y}^2} + \frac{\partial^2 C}{\partial \bar{x}^2}\right) \qquad (3)$$

Here, $\bar{x}$ and $\bar{y}$ are the local orthogonal coordinates with $\bar{x}$ along the tangent of the element, $\bar{u}$ and $\bar{v}$ are the corresponding velocity components, C is the species mass fraction, and D is the binary diffusivity which is assumed to be equal for both species. The local flowfield ($\bar{u}$, $\bar{v}$) can be directly related to the local strain field experienced about the material surfaces. The strain rates can be obtained from the flowfield given in Equation (2). If this flowfield produced a spatially uniform, time-dependent normal-strain field, then the second terms on both sides of Equation (3) could be eliminated. Furthermore, a material transformation given by

$$\zeta = \bar{y}e^{\int_0^t \epsilon(t')\,dt'}; \qquad \tau = \int_0^t \left[\exp\left(2\int_0^{t'} \epsilon(t'')\,dt''\right)\right] dt' \qquad (4)$$

can be invoked. Here, $\epsilon(t)$ is the time-dependent strain rate of the element along its tangent, ζ and τ are the stretched transverse distance and the transformed time accounting for the strain history of that particular element until it arrives to its current location. Under this transformation, Equation (3) reduces to the one-dimensional, unsteady, diffusion equation

$$\frac{\partial C}{\partial \tau} = D\frac{\partial^2 C}{\partial \zeta^2} \qquad (5)$$

with the appropriate initial and boundary conditions. For the case of C(y) > 0, t=0) = 1.0, C(y < 0, t=0) = 0.0, C(y → + ∞,t) = 1.0 and C(y → - ∞, t) = 0.0, the solution can be written in terms of the error function as

$$C = \frac{1}{2}\left[1 + \text{erf}\left(\frac{\zeta}{\sqrt{4D\tau}}\right)\right] \qquad (6)$$

In calculating the strain rates in the local orthogonal coordinate system $(\bar{x},\bar{y})$ attached to the material element, it is recognized that the local flowfield produces both a normal and a shear strain. While the normal strain component has a strong influence on the molecular diffusion across the material surface through steepening of the concentration gradients, the effect of shear strain on the diffusion process is much less significant. Therefore, the calculation of the strain rates for the solution of the diffusion equation can be based on the normal strain only. Until this point, much of the method of analysis follows that of Marble[8] and Marble and Karagozian[9]. In the determination of the concentration distribution about material surfaces, it is found that the diffusion zones surrounding the neighboring material surfaces overlap in the tightly-winded core region of the vortex. This effect becomes more pronounced as the Schmidt number (Sc = ν/D) decreases or the molecular diffusivity increases. This overlap is taken into account by superposition of the concentration profiles from neighboring regions. The superposition is admissable in view of the linearity of the transformed diffusion Equation (5). This permits the construction of the whole concentration field within the vortex from local concentration profiles at different locations within the vortex. Some error is introduced by the spatial variation of the strain rate, ϵ.

The concentration fields evaluated in this manner are subsequently used to determine the probability density distributions (pdf) from the concentration distribution along the x-direction at different y-positions utilizing Taylor's frozen flow hypothesis.

The periodicity in the x-direction allows the construction of pdf's from the concentration field within a single vortex in the row. In comparing the calculated pdf's with the experiments, some differences are expected due to the Lagrangian nature of the computations and the Eulerian nature of the experiments.

Chemically Reacting Vortex

Finite rate chemical reactions within a vortex are treated with a method based on Green's function solution of the reacting species conservation equation. The production terms in

the species conservation equations can be eliminated by the appropriate linear combination of these equations. This particular dependent variable, called the Schvab-Zel'dovich variable given by

$$C = \frac{\phi_{of} Y_f - Y_o + Y_{oi}}{Y_{oi} + \phi_{of} Y_{fi}} \qquad (7)$$

satisfies Equation (3) provided that the binary diffusivities are all equal. Here, Y's are mass fractions, ϕ_{of} is the stoichiometric oxidant to fuel mass ratio, subscripts, f, o and i refer to fuel, oxidant and initial respectively. In the simple case of a second-order finite-rate reaction between two species (fuel and oxidizer), only one of the species conservation equations needs to be solved and used along with the solution for the Schvab-Zel'dovich variable to determine completely the reacting scalar fields. The transformed fuel species equation under transformation in Equation (4) can be written as

$$\frac{\partial Y_f}{\partial \tau} = D \frac{\partial^2 Y_f}{\partial \zeta^2} + h(\tau) \frac{\dot{W}_f M_f}{\rho} \qquad (8)$$

Here, $h(\tau) = dt/d\tau$, and is related to the stretching, M_f and ρ are the fuel molecular weight and medium density respectively. Solution of Equation (8) can be obtained by the convolution of the appropriate Green's function[11,12]

$$G(\zeta,\tau|\zeta',\tau') = \frac{1}{\pi}\int_o^\infty e^{-D\alpha^2(\tau-\tau')} \cos\alpha(\zeta - \zeta')d\alpha \qquad (9)$$

The solution along a radial ray can be obtained if the layers of reactants within the vortex are treated as multiple strips of reaction layers undergoing straining. This permits determination of the fuel mass fraction distribution along a radial ray

$$Y_f(\zeta,\tau) = \frac{M_f}{\rho}\int_o^\tau \int_{-\infty}^{+\infty} W_f(\zeta',\tau')\, h(\tau')\, G(\zeta,\tau|\zeta',\tau')\, d\zeta' d\tau' + Y_f^o \qquad (10)$$

In this expression, Y_f^o is the solution for Y_f in the absence of chemical reactions. Thus, it corresponds to the pure diffusion. Solutions obtained along radial lines are used to construct the field of reacting scalars.

Solution of Equation (10) can be simplified since the Fourier form of the Green's function in Equation (7) suggests a form of Y_f given by

$$Y_f(\zeta,\tau) = \int_o^\infty f(\alpha,\tau)\cos\alpha\zeta\, d\alpha - \int_o^\infty g(\alpha,\tau)\sin\alpha\zeta\, d\alpha + Y_f^o \qquad (11)$$

where $f(\alpha,\tau)$ and $g(\alpha,\tau)$ are functions to be determined. After differentiating Equation (10) with respect to τ and comparing the resulting expression with the derivative of Equation (11), the following two integro-differential equations for f and g are obtained

$$\frac{\partial f}{\partial \tau} + D\alpha^2 f = \frac{M_f}{\rho\pi}\int_{-\infty}^{+\infty} W_f(\zeta',\tau)\, h(\tau)\cos\alpha\zeta' d\zeta' \qquad (12a)$$

$$\frac{\partial g}{\partial \tau} + D\alpha^2 g = \frac{M_f}{\rho\pi}\int_{-\infty}^{+\infty} W_f(\zeta',\tau)\, h(\tau)\sin\alpha\zeta' d\zeta' \qquad (12b)$$

They are subject to the initial conditions $f(\alpha,0) = 0$ and $g(\alpha,0) = 0$. In order to implement the solution, an approximation is made in Equation (11) by discretizing the continuous spectrum of α into discrete values from zero to a sufficiently large maximum value α_m. Equation (11) becomes

$$Y_f(\zeta,\tau) = \sum_n f_n(\alpha_n,\tau)\cos\alpha_n\zeta(\Delta\alpha) + \sum_n g_n(\alpha_n,\tau)\sin\alpha_n\zeta(\Delta\alpha) + Y_f^o \qquad (13)$$

provided that f_n and $g_n \to 0$ as $\alpha \to \alpha_m$. Under this approximation, Equations (12a) and (12b) transform to the following integro-differential equations:

$$\frac{df_n}{d\tau} + D\alpha_n^2 f_n = \frac{M_f}{\rho\pi}\int_{-\infty}^{+\infty} W_f(\zeta',\tau)\, h(\tau)\cos\alpha_n\zeta' d\zeta' \qquad (14a)$$

$$\frac{dg_n}{d\tau} + D\alpha_n^2 g_n = \frac{M_f}{\rho\pi}\int_{-\infty}^{+\infty} W_f(\zeta',\tau)\, h(\tau)\sin\alpha_n\zeta' d\zeta' \qquad (14b)$$

with $f_n(0) = 0$ and $g_n(0) = 0$. These equations are integrated by a second order Runge-Kutta method to determine the amplitude functions f_n and g_n.

The chemical reaction considered here is a second order, dilute isothermal reaction between NO and O_3. The reaction products are NO_2 and O_2 and both species are diluted in N_2. The reaction rate is taken from Givi et al[13], as

$$\frac{M_f W_f}{\rho} = -2.2 \times 10^5\, Y_{NO} Y_{O_3}\ \text{sec}^{-1} \qquad (15)$$

The initial mass fractions of the species were taken to be 0.01. In the next section, the results for reacting and nonreacting cases are discussed.

RESULTS

In this section, computed species mass fraction distributions and the corresponding probability density distributions within reacting and non-reacting row of vortices are presented for three cases. Figure 2 shows the distortion of an initially horizontal interface separating two species in the upper and lower planes in the presence of an infinite row of vortices. In this figure, the two species are immiscible (black and white). This vortex configuration simulates a shear layer between two streams of fluids with equal but opposite velocities. In our computations, we consider a reacting, gaseous shear layer containing ozone and nitric oxide as reactants. Both reactants are diluted in nitrogen so that the chemical reaction is isothermal. For the first two cases studied, ozone and nitric oxide with a mass fraction of 0.01 each occupy the upper and lower half-planes, respectively. In the third case, nitric oxide occupies the upper half plane with a mass fraction of 0.136 and ozone occupies the lower half-plane with a mass fraction of 0.01. This case simulates the reacting shear layer experiment of Masutani and Bowman[3].

The first case corresponds to a non-dimensional vortex strength (or vortex Reynolds number) $\Gamma/2\pi\nu$ of 50, a dimensionless time parameter, $\tau = 4\nu t/a^2$ of 0.02 and a Schmidt number, ν/D of unity. Figure 3 shows the normalized mass fraction of ozone across the vortex. The reacted core is surrounded by some excess ozone in the outer layer of the vortex as seen in Figure 2. The corresponding NO distribution is shown in Figure 4. It can be seen that some NO is still present in the reacted core because of the non-unity stoichiometry of the reaction (i.e. stoichiometric O_3 to NO mass ratio is 1.6). Figure 5 shows the distribution of the conserved scalar (mass fraction of the upper plane species for non-reacting case or the Schvab-Zel'dovich variable for reacting case) in the vortex. In the absence of chemical reactions, the vortex assumes a more diffused structure with lower concentration gradients compared to the reacting vortex. Figures 6 and 7 compare the probability density functions (pdf) for non-reacting and reacting cases respectively. For the non-reacting vortex, the pdf consists of two peaks at the unmixed concentrations (Y = 0.0 and Y = 1.0) as well as finite probabilites in the well-mixed core region around Y = 0.5. Chemical reactions alter the pdf by shifting the probability peaks at mixed concentrations to lower concentrations and by modifying the pdf peak at Y = 0.0. Both of these effects are due to the depletion of the species by finite rate chemical reactions.

The second case corresponds to a non-dimensional vortex strength of 125 and a time parameter of 0.004. These parameters simulate the conditions in the early part of reacting shear layer of Masutani and Bowman[3]. The vortex strength was computed based on the reported experimental conditions. The time parameter was estimated from the mean velocity at which the vortices are convected downstream and the location at which the comparisons were to be made (x = 11 cm). The ozone mass fraction distribution is depicted in Figure 8. The concentration field is less diffused and shows higher concentration gradients compared to the previous case. This is appropriate for a vortex with higher circulation at an early time in its growth. The higher vortex strength increases the concentration gradients through stretching. Figure 9 shows the NO concentration distribution within the vortex. The qualitative features of the distribution are similar to the previous case. The conserved scalar field, shown in Figure 10, appears to be somewhat different with steeper gradients. Therefore, it shows the vortex structure much more clearly.

The corresponding pdf's for reacting and non-reacting vortices are shown in Figures 11 and 12, respectively. Similar to the previous case, the effect of chemical reactions on the pdf is to modify the probability peak topography at zero-concentration of the reacting species and to reduce the probability peaks at the mixed concentrations. Figures 12 and 13 compare the computed and measured pdf's for the non-reacting shear layer experiment of Masutani and Bowman. Although the shape of the peaks at $C = 0.0$ and 1.0 are similar, the computations do not exhibit the experimentally observed "hump" on the high speed side of the mixing layer. In the Lagrangian frame of reference in which the computations are performed, the concentration field and the pdfs are antisymmetric about the x-axis. Therefore, these calculations are not expected to reproduce the "hump" observed in the experiments. This experimental observation is attributed to the higher rate of entrainment of the high-speed stream according to Dimotakis[15]. After relaxation of the frozen flow approximation, the antisymmetric character may no longer exist and this phenomenon can be studied theoretically.

In the measured pdfs reported by Masutani and Bowman[3] for the reacting mixing layer, the high-speed stream (upper plane) and the low-speed stream (lower plane) contained NO and O_3 respectively. The NO to O_3 mole fraction ratio in the free streams was 0.118 for one of the cases they studied. Computations were performed for this configuration to compare the pdf for the chemically reacting mixing layer. Figure 14 shows the computed NO mass fraction in the vortex. Figures 15 and 16 give a comparison of the experimentally determined and computed pdfs for the reacting species O_3. It should be noted that the shapes of the probability peaks are quite similar. Penetration of NO from the upper plane (high-speed stream) to the lower plane (low-speed stream) is a result of the abundance of NO in the upper half-plane. This causes the extension of the peak at Y = 0.0 to the lower half-plane. The same trend is found in the computations. It is also interesting to note that the "hump" observed for the non-reacting mixing layer has disappeared for the reacting case. This is believed to be simply due to the depletion of NO by the chemical reaction.

SUMMARY

Computation of species concentration distributions in non-reacting and reacting row of vortices have been presented for a few cases. It was shown that a piecewise analytical approach to the solution of molecular mixing and finite rate chemical reactions can be implemented to solve for the concentration fields. This method, first used by Marble[8], concentrates on the solution of mixing and reactions for a given flowfield.

Therefore, buoyancy effects and the influence of chemical reaction heat release on the flowfield are not considered. However, the technique avoids some of the numerical problems encountered in the full numerical simulations. The comparisons of the computed probability density functions with the experimentally determined pdfs show some encouraging agreements for the reacting case. For the non-reacting case, the computed pdf is antisymmetric whereas the measured pdf shows a mixing bias of the high-speed stream of the mixing layer. A complete parameter survey of Schmidt number, Reynolds number, and time is underway.

ACKNOWLEDGMENTS

The research reported in this paper was sponsred by Air Force Office of Scientific Research (AFOSR).

REFERENCES

1. Brown, G.L. and Roshko, A., "On the Density Effects and Large Structures in Turbulent Mixing Layers," J. Fluid Mech., 64, pp. 725-816 (1974).

2. Dimotakis, P.E. and Brown, G.L., "The Mixing Layer at High Reynolds Number: Large Structure Dynamics and Entrainment," J. Fluid Mech., 78, pp. 535-560 (1976).

3. Masutani, S.M. and Bowman, C.T., "Structure of a Chemically Reacting Mixing Layer," J. Fluid Mech., 172, pp. 92-126 (1986).

4. Konrad, J.H., "An Experimental Investigation of Mixing in 2D Turbulent Shear Flows with Application to Diffusion Limited Chemical Reactions," Ph.D. Thesis, California Institute of Technology, Pasadena, CA (1977).

5. Ghoniem, A.F. and Givi, P., "Vortex-Scalar Element Calculations of a Diffusion Flame," AIAA 25th Aerospace Sciences Meeting, AIAA-87-0225, Reno, Nevada (1987).

6. Lowery, P.S., Reynolds, W.C. and Mansour, N.M., "Passive Scalar Entrainment and Mixing in a Forced, Spatially-Developing Mixing Layer,: AIAA 25th Aerospace Sciences Meeting, AIAA-87-0132, Reno, Nevada (1987).

7. Lin, P. and Pratt, D.T., "Numerical Simulation of a Plane Turbulent Mixing Layer with Applications to Isothermal, Rapid Reactions," AIAA 25th Aerospace Sciences Meeting, AIAA-87-1224, Reno, Nevada 91987).

8. Marble, F.E., "Growth of a Diffusion Flame in the Field of a Vortex," Recent Advances in the Aerospace Sciences, Paper No. 19, pp. 395-413, Editor: Corrado Casci, Plenum Publishing Corporation (1985).

9. Kargozian, A.K. and Marble, F.E., "Study of a Diffusion Flame in a Stretched Vortex," Combustion Science and Technology, Vol. 45, pp. 65-84 (1986).

10. Categen, B.M. and Sirignano, W.A., "Study of Mixing and Reaction in the Field of a Vortex," Joint Meeting of the Combustion Institute Western States and Japanese Section, Paper No. 3B-44, Honolulu, Hawaii (1987).

11. Lamb, B. Hydrodynamics, Sixth Edition (1932) Dover Publications, New York.

12. Morse, P.M. and Feshbach, H., Methods of Theoretical Physics, Parts I and II, McGraw-Hill (1953).

13. Carslaw, H.S. and Jaeger, J.C., Conduction of Heat in Solids, Chapter XIV, Oxford: Clarnedon Press (1959).

14. Givi, P., Ramos, J.I., and Sirignano, W.A., "Probability Density Function Calculations in Turbulent Chemically Reacting Round Jets, Mixing Layers and One-Dimensional Reactors," J. Non-Equilib. Thermodyn., Vol. 10, pp. 75-104 (1985).

15. Dimotakis, P.W., "Entrainment into a Fully-Developed Two-Dimensional Shear Layer," AIAA Paper No. 84-0368 (1984).

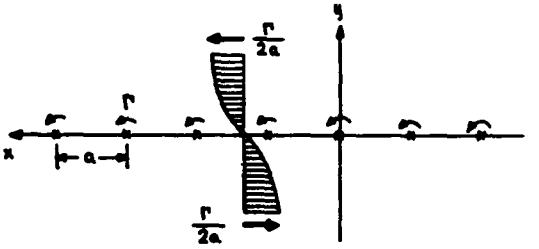

Figure 1. Infinite Vortex Row Configuration.

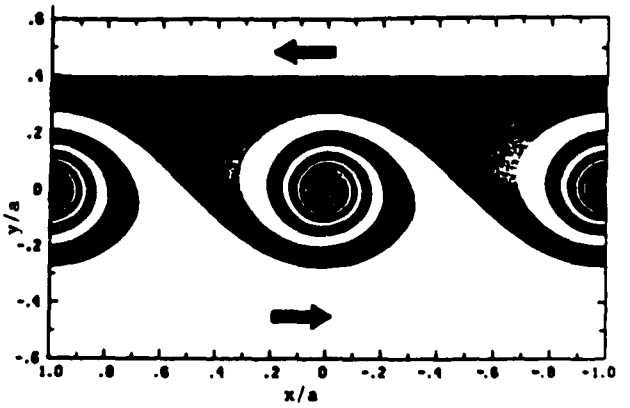

Figure 2. Distortion of an initially horizontal interface Re = 50, τ = 0.02.

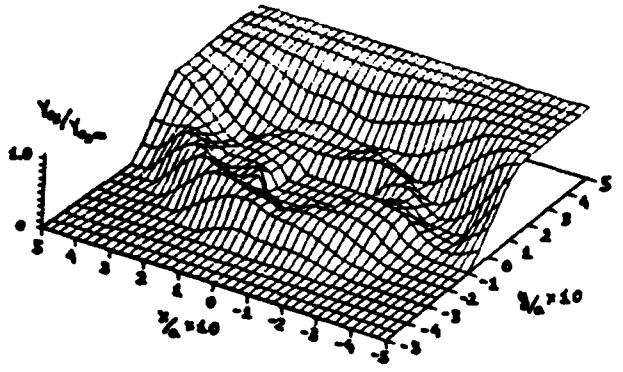

Figure 3. O_3 mass fraction for Re = 50, τ = 0.02, Sc = 1.0.

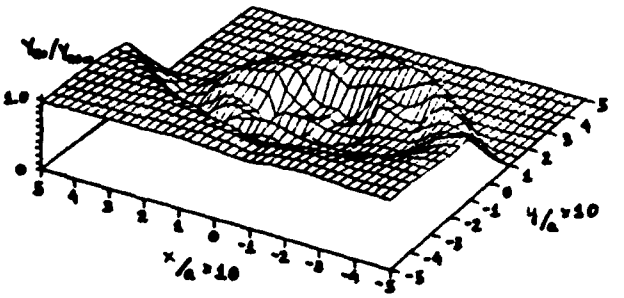

Figure 4. NO mass fraction for Re = 50, τ = 0.02, Sc = 1.0.

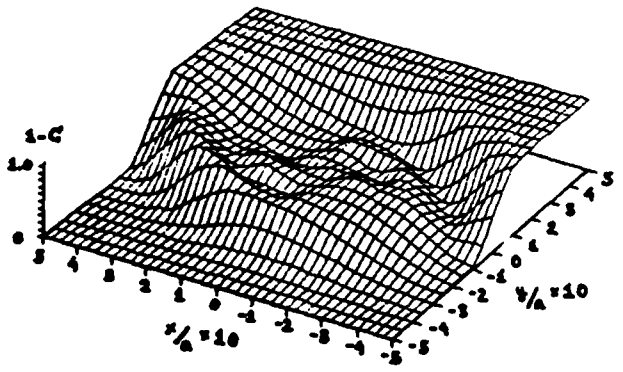

Figure 5. Conserved scalar mass fraction for Re = 50, τ = 0.02 and Sc = 1.0.

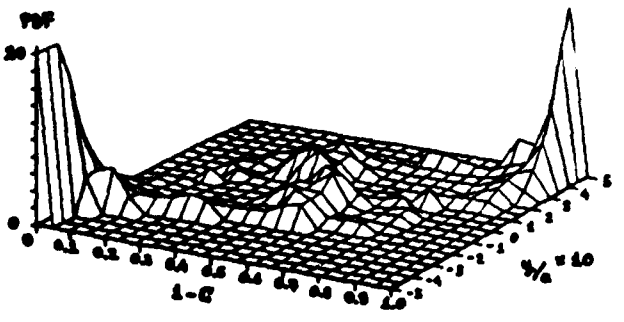

Figure 6. Probability density of conserved scalar for Re = 50, τ = 0.02, Sc = 1.0.

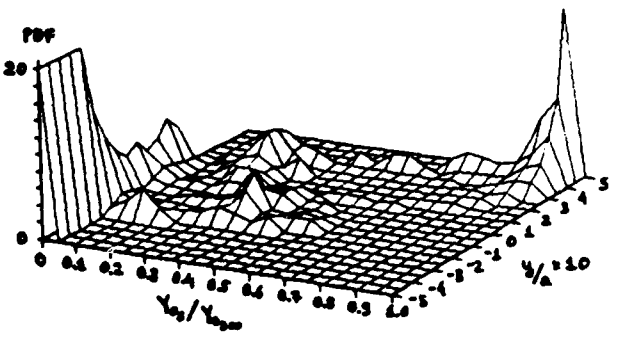

Figure 7. Probability density of reacting O_3 species for Re = 50, τ = 0.02.

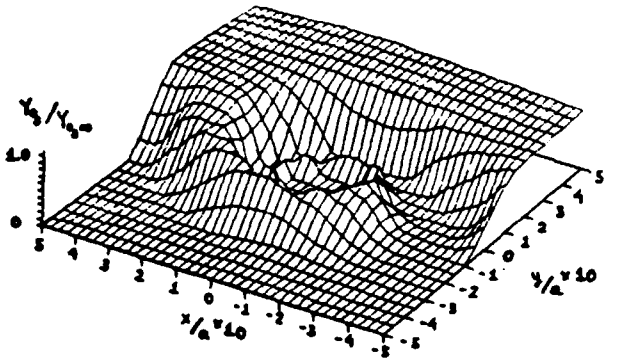

Figure 8. O_3 mass fraction for Re = 125, τ = 0.004 and Sc = 1.0.

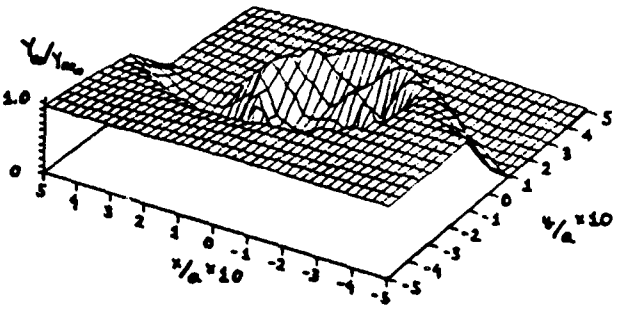

Figure 9. NO mass fraction for Re = 125, τ = 0.004 and Sc = 1.0.

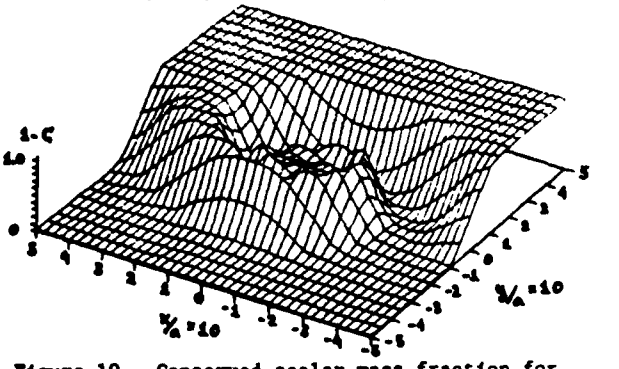

Figure 10. Conserved scalar mass fraction for Re = 125, τ = 0.004 and Sc = 1.0.

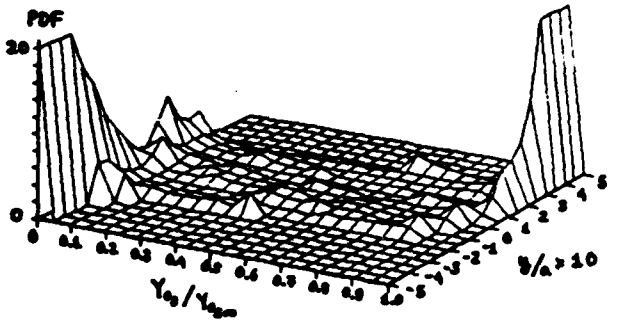

Figure 11. Probability density of reacting O_3 species for Re = 125, τ = 0.004 and Sc = 1.0.

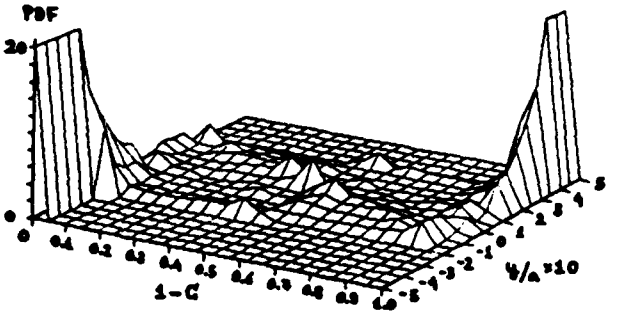

Figure 12. Probability density of conserved scalar for Re = 125, τ = 0.004 and Sc = 1.0.

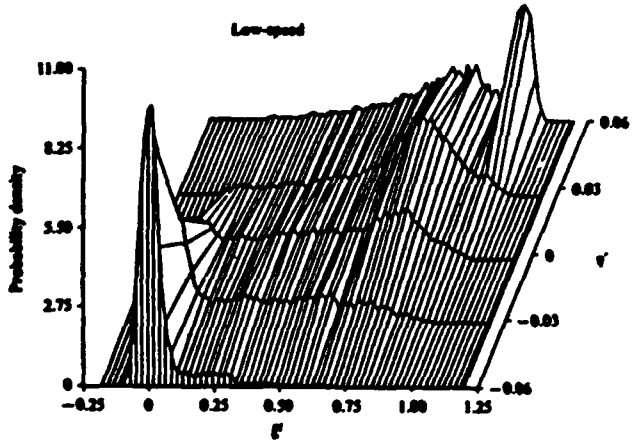

Figure 13. Probability density for the non-reacting shear layer of Masutani & Bowman at x = 11cm. O_3 is in the high speed stream.

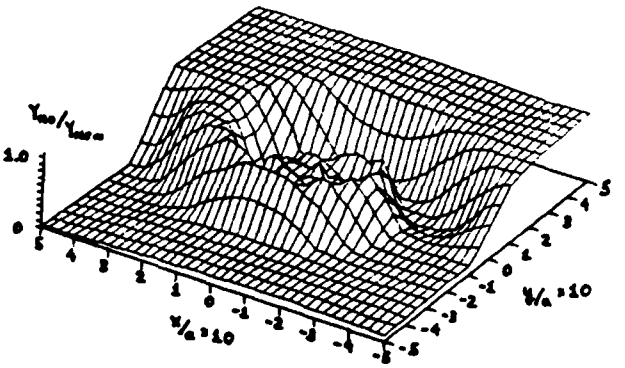

Figure 14. NO mass fraction for the simulated shear layer of Masutani and Bowman. NO is in the high speed stream (upper half-plane)

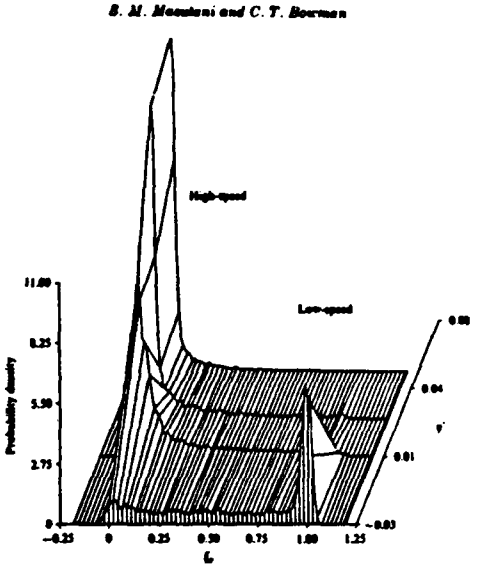

Figure 15. Probability density of O_3 measured in the reacting shear layer of Masutani and Bowman for a molar O_3 to NO stoichiometry of .118. NO is in the high-speed stream.

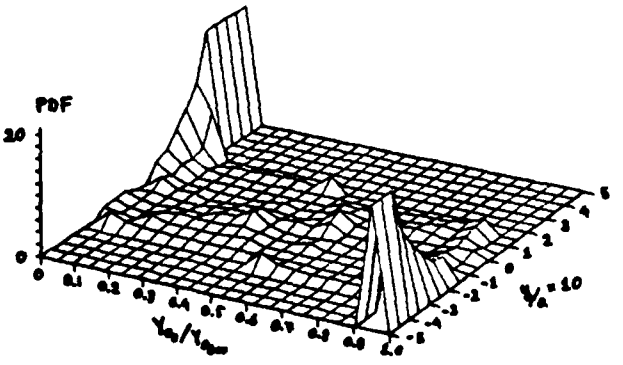

Figure 16. Probability density of O_3 in the simulated Masutani & Bowman experiment (conditions of Figure 15).

END
DATE
FILMED
5-88
DTIC